



## OPEN ACCESS

## EDITED BY

Ayad Faqi,  
Soran University, Iraq

## REVIEWED BY

Peng Li,  
SINOPEC Petroleum Exploration and  
Production Research Institute, China  
Muhammed Omer,  
Salahaddin University, Iraq

## \*CORRESPONDENCE

Hao Li,  
✉ lihaowyc@163.com

RECEIVED 18 June 2024

ACCEPTED 11 October 2024

PUBLISHED 29 October 2024

## CITATION

Wang Y, Li H, Mou C, Chen W, Gao C, Liang W,  
Zheng B, Hou Q and Xia Y (2024) Sedimentary  
characteristics and evolution of the Upper  
Permian Wujiaping Formation in the eastern  
Yangtze Block.

*Front. Earth Sci.* 12:1450872.

doi: 10.3389/feart.2024.1450872

## COPYRIGHT

© 2024 Wang, Li, Mou, Chen, Gao, Liang,  
Zheng, Hou and Xia. This is an open-access  
article distributed under the terms of the  
[Creative Commons Attribution License \(CC  
BY\)](https://creativecommons.org/licenses/by/4.0/). The use, distribution or reproduction in  
other forums is permitted, provided the  
original author(s) and the copyright owner(s)  
are credited and that the original publication  
in this journal is cited, in accordance with  
accepted academic practice. No use,  
distribution or reproduction is permitted  
which does not comply with these terms.

# Sedimentary characteristics and evolution of the Upper Permian Wujiaping Formation in the eastern Yangtze Block

Yuanhong Wang<sup>1,2</sup>, Hao Li<sup>3\*</sup>, Chuanlong Mou<sup>4</sup>, Weiwei Chen<sup>4</sup>,  
Chang Gao<sup>4</sup>, Wei Liang<sup>4</sup>, Binsong Zheng<sup>2,5</sup>, Qian Hou<sup>4</sup> and  
Yu Xia<sup>4</sup>

<sup>1</sup>School of Electronic Information and Engineering, Yangtze Normal University, Chongqing, China, <sup>2</sup>Key Laboratory of Sedimentary Basin and Oil and Gas Resources, Ministry of Natural Resources, Chengdu, China, <sup>3</sup>Wuxi Research Institute of Petroleum Geology, SINOPEC, Wuxi, China, <sup>4</sup>Chengdu Centre of China Geological Survey, Chengdu, China, <sup>5</sup>School of Geoscience and Technology, Southwest Petroleum University, Chengdu, China

The Upper Permian Wujiaping (WJP) Formation in the Yangtze Block (Southern China) has great potential for shale gas exploration. However, the sedimentary characteristics and environmental evolution of the WJP Formation are poorly understood. Based on 260 hand specimen samples obtained from 18 sections and 1 borehole in the eastern Yangtze Block, petrographic observations reveal that the WJP Formation is composed of 11 rock types. Combined with analyses of geochemical compositions, the sedimentary facies belts of the WJP Formation are divided into shoreland, shallow-water shelf, deep-water shelf shoal, restricted platform, and open platform. Bauxite was developed in the shoreland at the bottom of the WJP Formation, which is attributed to the Dongwu movement. The formation of paleo-uplift exerted a significant effect on paleogeomorphology and led to a major change in the sedimentary model from the underlying stratum to the WJP Formation. During the lower WJP Formation sedimentary period, gradual transgression occurred in the eastern Yangtze Block, and the lithology was mainly composed of clastic rocks. Shoreland, shallow-water shelf, and deep-water shelf were developed northeastward in turn. In the period of the upper WJP Formation, due to durative transgression, the area of the shoreland reduced southwestward. The lithology converted from clastic rocks into carbonates, and the restricted platform and open platform were developed northeastward. A few patched shoals formed in the restricted platform.

## KEYWORDS

sedimentary evolution, geochemical analysis, the Dongwu movement, the Wujiaping Formation, eastern Yangtze Block

## 1 Introduction

The Upper Permian is one of the most important source rocks in the Paleozoic of the Yangtze Block in South China (Chai, 2019; Liang and Li, 2021). The lower member of the Wujiaping (WJP) Formation is considered to have good potential in

shale gas exploration and development (Liang et al., 2008). Focusing on the shale of the Wujiaping Formation, a large number of exploration practices have been carried out in the past 10 years in the southern Yangtze Block (Zhou et al., 2012; Zhang et al., 2014; Zhang et al., 2013; Luo and He, 2014; Wang et al., 2014; Gu et al., 2015; Li G. L. et al., 2015; Li J. et al., 2015; Liu et al., 2015; Jiang et al., 2019; Hu et al., 2020; Wang et al., 2015). Regarding the eastern Yangtze Block, early studies have shown that the Upper Permian Wujiaping Formation has gas accumulation conditions, but its shale gas prospects are still unclear, which is mainly due to the poor understanding of the sedimentary characteristics and evolution of the WJP Formation (Fan, 2016; Cai, 2017; Lin et al., 2009; Zhao et al., 2012). Regarding the development of shoreland and tidal flats at the bottom of the Wujiaping Formation, scholars have reached an agreement (Zhao et al., 2012; Liu et al., 2010; Tian et al., 2010). However, regarding the rest of the Wujiaping Formation, some researchers considered it the middle ramp (Lin et al., 2009), while others prefer the open platform (Zhao et al., 2012; Tian et al., 2010). In addition, although researchers noted the development of the bauxite and aluminous clay rocks at the bottom of the Wujiaping Formation, its distribution and geological meanings have been ignored. Moreover, in order to broaden the exploration of shale gas, researchers conducted a survey of the sedimentary environments, total organic carbon (TOC), distribution, maturity of organic matter, and type of organic matter of the carbonaceous mudstone (Teng et al., 2010; Cai, 2017; Cao et al., 2018; Zhao et al., 2012; Liu et al., 2010; Tian et al., 2010) while ignoring the effects of the paleoclimate, redox conditions, and hydrodynamic conditions on the organic accumulation. Based on these, the analysis of petrology and geochemical data, the rock types, sedimentary environment, and sedimentary evolution of the Wujiaping Formation on the eastern Yangtze Block was carried out in this paper to provide a geological basis for the exploration of shale gas resources in the Wujiaping Formation.

## 2 Geologic settings

The study area is located in the Yangtze Block, bordered by the Qinling orogenic belt to the north and the Jiangnan–Xuefeng uplift to the east (Figure 1A). Controlled by tectonic movements, the study area experienced a craton basin in Caledonian (N<sub>h</sub>-O<sub>1</sub>), foreland uplift basin (O<sub>2</sub>-S), craton basin in Hercynian and Early Indosinian (D-T<sub>2</sub>), foreland basin in Late Indosinian and Early Yanshan (T<sub>3</sub>-J<sub>2</sub>), intense fold deformation in Early Yanshan (J<sub>3</sub>-K<sub>1</sub>), extensional basin in Late Yanshan and Early Himalayan (K<sub>2</sub>-E), and intense compression and deformation in Late Himalayan (N-Q).

In the Early Permian, due to the tectonic subsidence, most areas of the eastern Yangtze Block were rapidly and extensively transgressed. However, the differential uplifting movement of crust at the end of the Early Permian, called the Dongwu movement, resulted in different degrees of denudation at the top of the Maokou Formation. In the Late Permian, with the opening of the Paleo–Tethys Ocean, large-scale intracontinental rifting occurred in the Middle and Upper Yangtze Block. The seawater invaded from east to west. Through the multi-stage transformation of the

structural system during the Triassic to Quaternary, currently, the study area is located between the fault–fold belts and the uplift belts (Figure 1B).

## 3 Samples and analytical methods

### 3.1 Sample collection and handling

A total of 260 hand specimen samples were obtained from 18 sections and 1 well in the study area (Figure 1C). Thin sections with a thickness of 0.03 mm were prepared from all samples and impregnated with blue dye to recognize porosity. The thin sections of carbonates were stained using Alizarin Red S in one-third of the region to distinguish calcite and dolomite.

All the rock samples were air-dried and finely ground to a 200 mesh size for geochemical analysis. Major and trace elements were measured in the Key Laboratory of Sedimentary Basin and Oil and Gas Resources, Ministry of Natural Resources, Chengdu, China. Major elements were analyzed using an X-ray fluorescence spectrometer (PW2404). Loss on ignition (LOI) was estimated by heating the sample at 1,000°C for 90 min and recording the weight loss. The analytical accuracy errors of the major element data were generally less than 5%. Trace elements were determined using an Element XR inductively coupled plasma mass spectrometer (ICP-MS). Then, 50 mg samples were dissolved in a mixed solution of HClO<sub>4</sub>, HF, and HNO<sub>3</sub>. The analytical uncertainty was usually less than 5%.

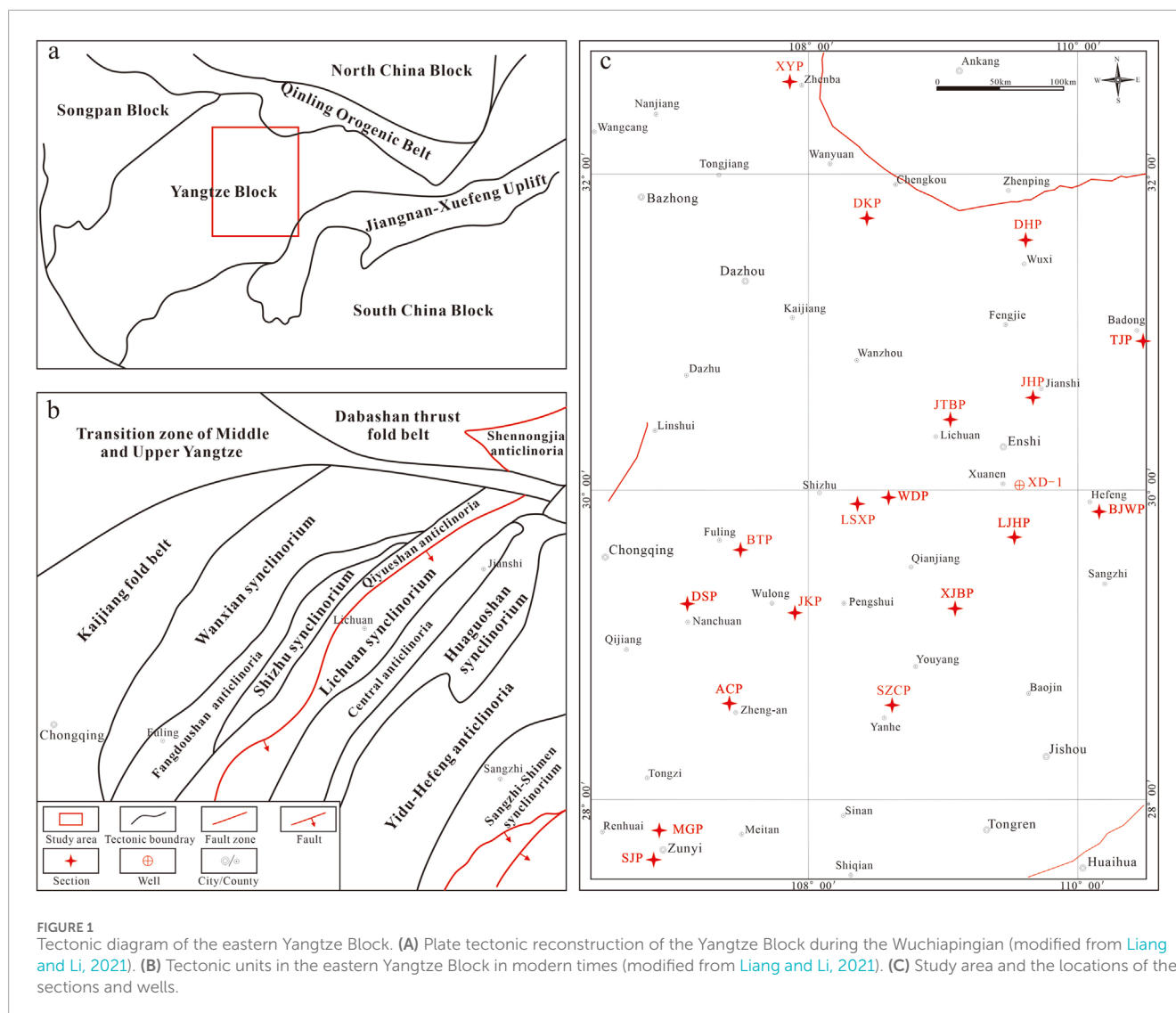
### 3.2 Analytical methods

In order to rebuild the sedimentary environment of the WJP Formation in the study area, the paleoclimate, redox conditions, and hydrodynamic conditions of the Wujiaping Formation are discussed in this article.

#### 3.2.1 Analytical method for paleoclimate

The paleoclimate of the Wujiaping Formation is inferred from the chemical index of alteration (CIA).

The CIA is often applied to determine the degree of chemical weathering and the climate (Nesbitt and Young, 1982). Normally, if the CIA values range from 80 to 100, it is suggestive of a hot and humid climate with intensive chemical weathering. If the CIA values are between 60 and 80, it reflects a warm and humid climate with medium chemical weathering. The low CIA values (50–60) reveal a cold and arid climatic condition with weak chemical weathering (Fedo et al., 1995; Yan et al., 2010; Fu et al., 2015; Ma et al., 2015). The CIA is obtained from the following equation:  $CIA = 100 \times [Al_2O_3 / (Al_2O_3 + CaO^* + Na_2O + K_2O)]$ , where the major element concentrations are presented as molecular proportions and CaO\* is defined as the concentration of CaO present in the silicate fraction only. McLennan (1993) pointed out that the CaO\* values followed the following rules: CaO values were accepted only if  $CaO < Na_2O$ ; and if  $CaO > Na_2O$ , it was assumed that the concentration of CaO is equal to that of Na<sub>2</sub>O.



### 3.2.2 Analytical method for redox conditions

Redox conditions in the Wujiaping Formation are indicated by the index of trace elements.

Mo and U are the trace elements most sensitive to changes in seawater redox conditions (Tribouillard et al., 2012; Algeo and Tribouillard, 2009). First, the content of Mo and U is very low in continental upper crust and clastic sediments. They are enriched in seawater and remain inactive in the oxidizing environment, making them easily precipitate in sediments in the anoxic environment. Based on the different enrichment processes of Mo and U in sediments, the U enrichment factor (EF)–Mo enrichment factor covariant maps are proposed to interpret redox conditions. With the increase in the reduction in the bottom water, the enrichment degree of U and Mo increases, and the rate of enrichment of Mo is faster than that of U. Thus, the ratio of  $Mo_{EF}/U_{EF}$  increases with the increase in the reduction in seawater (Wedepohl, 1971; Wedepohl, 1991). In this article, the EF was used to quantitatively describe the enrichment degree of Mo and U elements. The EF is calculated based on the average shale component. The formula is  $EF_{element}$

$= (\text{element}/Al)_{\text{sample}} / (\text{element}/Al)_{\text{average shale}}$  (Brumsack, 2006; Ross and Bustin, 2009).

### 3.2.3 Analytical method for hydrodynamic conditions

Zr elements are often enriched in heavy minerals of sandstone in coastal environments and rare in clay minerals of mudstone in deep marine environments. On the contrary, Rb elements are often enriched in light minerals such as clay and mica in deep marine environments. Thus, the Zr/Rb ratio can quantify the relative strength of the hydrodynamic conditions. The higher the Zr/Rb ratio is, the stronger the hydrodynamic conditions of sedimentary environments are (Liu et al., 2002).

## 4 Results

Through the observations from hand specimen samples and thin sections, 11 rock types of the Wujiaping Formation are classified (Table 1).

TABLE 1 Rock types of the Wujiaping Formation in the region of the eastern Yangtze Block.

Rock type	Thin-section photography	Size of grains	Description	Water energy	Depositional environment
Bauxite	Figures 2A–D	Silt to fined	A large number of aluminous minerals and clay can be seen, and oolitic structures are also developed	High	Shoreland
Siliceous rock	Figure 2E	Mud (matrix)	Black–gray and lamellar structure	Low	Deep-water shelf
Argillaceous siltstone	Figure 2F	Mud (matrix) Silt	Faint yellow, a few interlayers of gray mudstone	Low to medium	Shoreland
Carbonaceous mudstone	Figures 2G,H	Mud (matrix)	Black, plenty of horizontal beddings	Low	Marsh of shoreland
Siliceous mudstone	Figure 2I	Mud (matrix) Silt (siliceous radiolarian)	A few siliceous radiolarian	Low	Deep-water shelf
Bioclastic mudstone	Figure 2J	Mud (matrix) Silt to medium (bioclasts)	Plenty of fragments of brachiopod and echinoderm (such as crinoid)	Low	Shoreland
Micrite	Figure 2K	Micrite (calcite)	Micrite calcite, no obvious sedimentary structures	Low	Deep-water shelf and shallow-water shelf
Calcsphere limestone	Figure 2L	Micrite (matrix) Silt to fined (calcsphere)	Plenty of calcsphere, ellipsoidal to rounded	Medium	Shallow-water shelf and restricted platform
Bioclastic limestone	Figure 2M	Micrite to fined (cementation) fined to medium (bioclasts)	Plenty of bioclasts	Medium to high	Shoal
Bioclastic micrite	Figure 2N	Micrite (cementation) Fined to medium (bioclasts)	Fes bioclasts	Low to medium	Restricted platform
Chert nodule and clot limestone	Figure 2O	Micrite (matrix)	Chert nodules and clots, with sizes 4–8 cm and 5–16 cm, respectively	Low	Deep-water shelf and shallow-water shelf

## 4.1 Lithologic composition

### 4.1.1 Bauxite

Bauxite is composed of hydroxides and oxides, commonly known as gibbsite, boehmite, and diaspor. Bauxite and aluminous clay rock are developed in the study area. Macroscopically, bauxite is usually flesh red and brown, with no obvious stratification (Figure 2A). Microscopically, a large number of aluminous minerals and clay are observed, and oolitic structures are also developed (Figures 2B–D).

### 4.1.2 Siliceous clastic rocks

The siliceous clastic rocks in the WJP Formation are divided into siliceous rocks and argillaceous siltstones. Siliceous rocks in the study area are mainly developed at P<sub>3</sub>W<sub>1</sub> while also found in

P<sub>3</sub>W<sub>2</sub> in some areas like well XD-1, JTBP in Lichuan, DKP in Xuanhan, and XJBP in Laifeng. At the macro-scale, siliceous rocks are characterized by a black–gray lamellar structure (the thickness of each lamina is less than 10 cm; Figure 2E).

Argillaceous siltstones in the Wujiaping Formation are mainly developed at P<sub>3</sub>W<sub>1</sub>. At the macro-scale, the argillaceous siltstone is grayish yellow and faint yellow, with a few interlayers of gray mudstone (Figure 2F).

### 4.1.3 Mudstone

The mudstone in the study area is composed of carbonaceous mudstone, siliceous mudstone, and bioclastic mudstone.

At the macro-scale, carbonaceous mudstone in the Wujiaping Formation is characterized by black–gray or black, and plenty of horizontal beddings can be found (Figures 2G, H). Usually,

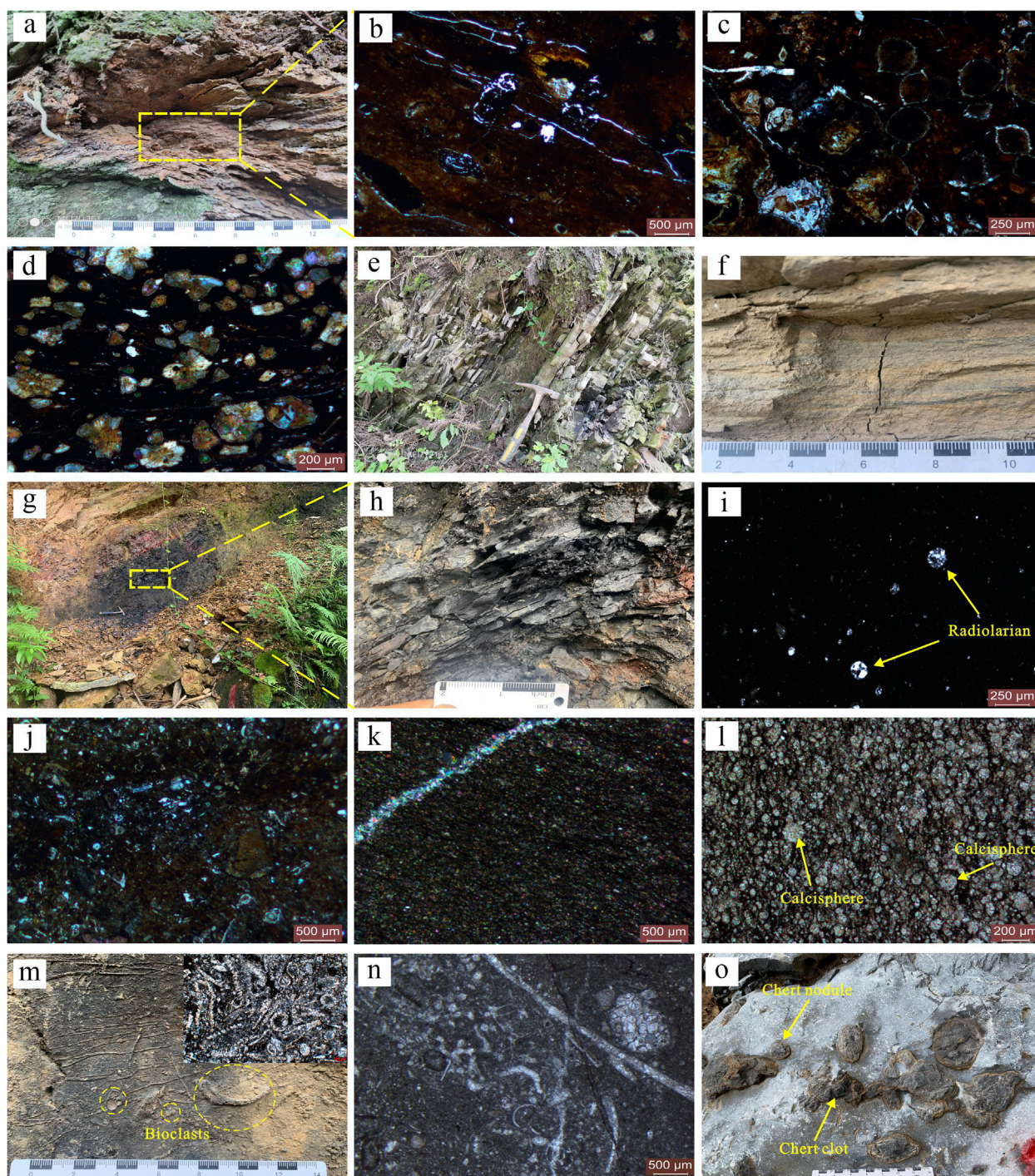


**FIGURE 2**

Macroscopic and microscopic characteristics of rock types in the Wujiaping Formation in the eastern Yangtze Block. **(A)** Bauxite,  $P_3W_1$ , LSXP. **(B)** Bauxite,  $P_3W_1$ , LSXP. **(C)** Bauxite,  $P_3W_1$ , well XD-1. **(D)** Aluminous clay rock,  $P_3W_1$ , well XD-1. **(E)** Siliceous rock,  $P_3W_1$ , LSXP. **(F)** Argillaceous siltstone,  $P_3W_1$ , LSXP. **(G)** Carbonaceous mudstone,  $P_3W_1$ , JHP. **(H)** Carbonaceous mudstone,  $P_3W_1$ , JHP. **(I)** Siliceous mudstone, radiolarian,  $P_3W_1$ , LSXP. **(J)** Bioclastic mudstone,  $P_3W_1$ , DSP. **(K)** Micrite,  $P_3W_2$ , JTBP. **(L)** Calcisphere limestone,  $P_3W_2$ , DKP. **(M)** Bioclastic limestone,  $P_3W_2$ , SZCP. **(N)** Bioclastic limestone,  $P_3W_2$ , JKP. **(O)** Chert nodule and clot limestone,  $P_3W_2$ , DKP.

carbonaceous mudstone is mainly distributed at the lower part of  $P_3W_1$ , and its stratification is inconspicuous.

Siliceous mudstone is mainly developed at  $P_3W_1$ , which is usually accompanied by siliceous rocks. At

the macro-scale, siliceous mudstone is characterized by black-gray and rare beddings. Microscopically, some siliceous radiolarians can be found in siliceous mudstone (Figure 2I).

TABLE 2 Major elements of the Wujiaoping Formation in the region of the eastern Yangtze Block.

Sample	Formation	SiO <sub>2</sub> (%)	Al <sub>2</sub> O <sub>3</sub> (%)	CaO (%)	MgO (%)	K <sub>2</sub> O (%)	Na <sub>2</sub> O (%)	TiO <sub>2</sub> (%)	P <sub>2</sub> O <sub>5</sub> (%)	MnO (%)	Fe <sub>2</sub> O <sub>3</sub> (%)	CIA
XD-1-HF1	P <sub>3</sub> W <sub>1</sub>	29.22	18.30	1.32	2.74	1.80	0.40	2.30	0.12	0.44	28.68	84.84
XD-1-HF2	P <sub>3</sub> W <sub>1</sub>	19.87	16.16	0.86	1.73	0.97	0.49	3.56	0.14	0.16	42.00	85.84
XD-1-HF3	P <sub>3</sub> W <sub>1</sub>	50.98	16.18	3.26	1.27	1.70	2.37	2.04	0.32	0.05	4.84	62.66
XD-1-HF4	P <sub>3</sub> W <sub>1</sub>	45.77	14.69	5.90	2.03	1.44	2.41	1.80	0.23	0.09	7.10	60.75
XD-1-HF5	P <sub>3</sub> W <sub>1</sub>	47.18	18.52	4.79	1.77	1.98	2.46	2.22	0.30	0.07	5.64	64.39
XD-1-HF6	P <sub>3</sub> W <sub>1</sub>	34.21	12.33	17.79	0.91	0.75	4.46	1.58	0.21	0.07	5.33	44.32
XD-1-HF7	P <sub>3</sub> W <sub>1</sub>	49.42	17.34	2.33	1.47	2.31	1.45	1.98	0.22	0.15	7.93	70.44
XD-1-HF8	P <sub>3</sub> W <sub>1</sub>	52.04	17.28	3.33	1.70	2.52	1.13	2.15	0.13	0.06	5.66	72.81
XD-1-HF9	P <sub>3</sub> W <sub>1</sub>	56.92	15.93	2.67	1.38	2.31	1.22	2.01	0.13	0.05	4.57	70.96
XD-1-HF10	P <sub>3</sub> W <sub>1</sub>	73.30	7.40	5.19	0.40	0.92	1.32	0.56	0.33	0.02	1.21	58.08
XD-1-HF11	P <sub>3</sub> W <sub>2</sub>	54.08	15.86	5.33	1.52	1.95	3.11	1.46	0.18	0.07	3.74	56.22
XD-1-HF12	P <sub>3</sub> W <sub>2</sub>	20.77	1.72	40.10	0.65	0.06	0.75	0.07	0.04	0.11	1.09	40.41
XD-1-HF13	P <sub>3</sub> W <sub>2</sub>	64.30	2.08	15.80	0.65	0.28	0.34	0.07	0.03	0.02	0.30	59.39
XD-1-HF14	P <sub>3</sub> W <sub>2</sub>	8.56	1.44	48.03	0.64	0.09	0.48	0.05	0.03	0.03	0.43	46.26
XD-1-HF15	P <sub>3</sub> W <sub>2</sub>	21.85	3.39	36.70	2.00	0.44	0.62	0.14	0.03	0.03	0.82	57.39
XD-1-HF16	P <sub>3</sub> W <sub>2</sub>	5.50	1.92	48.53	0.62	0.08	0.78	0.02	0.03	0.03	0.19	41.96
XD-1-HF17	P <sub>3</sub> W <sub>2</sub>	83.52	0.056	6.22	0.43	0.03	0.07	0.01	0.04	0.01	0.058	17.74
JTBP-HF1	P <sub>3</sub> W <sub>1</sub>	83.50	3.80	0.63	0.32	0.66	0.21	0.16	0.08	<0.01	1.39	72.98
JTBP-HF2	P <sub>3</sub> W <sub>1</sub>	59.03	19.68	0.35	1.77	4.37	0.59	0.74	0.17	0.12	5.10	76.88
JTBP-HF3	P <sub>3</sub> W <sub>1</sub>	68.84	7.68	1.39	0.52	1.72	0.60	0.30	1.33	<0.01	2.40	79.25
JTBP-HF4	P <sub>3</sub> W <sub>1</sub>	75.52	6.29	0.11	0.37	1.14	0.58	0.23	0.05	0.01	4.25	73.53
JTBP-HF5	P <sub>3</sub> W <sub>1</sub>	72.73	6.20	0.11	0.34	1.12	0.64	0.23	0.12	0.02	6.28	74.13
JTBP-HF6	P <sub>3</sub> W <sub>1</sub>	72.03	8.76	0.88	0.55	1.95	0.65	0.32	0.53	<0.01	2.50	71.78

(Continued on the following page)

TABLE 2 (Continued) Major elements of the Wujaping Formation in the region of the eastern Yangtze Block.

Sample	Formation	SiO <sub>2</sub> (%)	Al <sub>2</sub> O <sub>3</sub> (%)	CaO (%)	MgO (%)	K <sub>2</sub> O (%)	Na <sub>2</sub> O (%)	TiO <sub>2</sub> (%)	P <sub>2</sub> O <sub>5</sub> (%)	MnO (%)	Fe <sub>2</sub> O <sub>3</sub> (%)	CIA
JTBP-HF7	P <sub>3</sub> W <sub>1</sub>	64.32	9.34	1.16	0.53	1.76	0.71	0.36	0.64	0.01	5.18	72.36
JTBP-HF8	P <sub>3</sub> W <sub>1</sub>	64.88	9.20	0.42	0.62	2.03	0.50	0.39	0.05	<0.01	1.19	71.52
JTBP-HF9	P <sub>3</sub> W <sub>1</sub>	59.82	11.61	0.31	0.80	2.56	0.21	0.50	0.10	<0.01	2.56	77.17
JTBP-HF10	P <sub>3</sub> W <sub>1</sub>	75.33	9.39	0.42	0.49	1.90	0.25	0.30	0.06	<0.01	2.66	76.50
JTBP-HF11	P <sub>3</sub> W <sub>1</sub>	84.08	4.52	0.36	0.24	0.74	0.45	0.14	0.07	0.01	1.32	68.96
JTBP-HF12	P <sub>3</sub> W <sub>1</sub>	68.62	10.12	1.01	0.58	2.01	0.46	0.37	0.07	<0.01	2.41	73.26
JTBP-HF13	P <sub>3</sub> W <sub>1</sub>	89.91	1.85	0.07	0.11	0.26	0.42	0.09	0.02	<0.01	0.54	63.80
JTBP-HF14	P <sub>3</sub> W <sub>1</sub>	77.73	5.77	0.10	0.36	1.29	0.54	0.28	0.02	<0.01	0.46	70.46
JTBP-HF15	P <sub>3</sub> W <sub>1</sub>	76.94	5.42	0.06	0.28	1.30	0.50	0.28	0.02	<0.01	0.45	70.28
JTBP-HF16	P <sub>3</sub> W <sub>1</sub>	31.56	0.98	22.07	12.15	0.18	0.14	0.04	0.04	0.07	0.41	59.90
JTBP-HF17	P <sub>3</sub> W <sub>1</sub>	59.14	4.23	14.63	0.96	0.41	1.53	0.14	0.07	0.04	1.55	43.57
JTBP-HF18	P <sub>3</sub> W <sub>1</sub>	47.66	4.43	19.83	0.53	0.50	1.54	0.14	0.06	0.02	1.66	44.13
JTBP-HF19	P <sub>3</sub> W <sub>2</sub>	45.41	3.45	21.78	1.01	0.77	0.46	0.13	0.23	0.02	1.70	59.49
JTBP-HF20	P <sub>3</sub> W <sub>2</sub>	13.24	1.41	40.60	4.50	0.24	0.25	0.05	0.04	0.04	0.54	56.56
JTBP-HF21	P <sub>3</sub> W <sub>2</sub>	17.58	1.30	41.64	1.70	0.20	0.34	0.04	0.03	0.05	0.63	49.32
JTBP-HF22	P <sub>3</sub> W <sub>2</sub>	26.46	2.68	28.68	7.66	0.60	0.08	0.09	0.05	0.07	1.15	74.56
JTBP-HF23	P <sub>3</sub> W <sub>2</sub>	18.75	1.41	41.98	0.69	0.28	0.24	0.05	0.04	0.02	0.48	56.32
JTBP-HF24	P <sub>3</sub> W <sub>2</sub>	18.25	0.86	42.38	0.74	0.12	0.23	0.03	0.09	0.02	0.51	49.23
JTBP-HF25	P <sub>3</sub> W <sub>2</sub>	5.83	0.70	43.32	7.20	0.14	0.03	0.04	0.07	0.01	0.27	73.64
JTBP-HF26	P <sub>3</sub> W <sub>2</sub>	35.53	0.70	33.83	0.44	0.16	0.04	0.02	0.05	0.01	0.17	69.64
JTBP-HF27	P <sub>3</sub> W <sub>2</sub>	29.04	0.96	35.18	2.50	0.22	0.04	0.04	0.10	0.02	0.32	72.16
JTBP-HF28	P <sub>3</sub> W <sub>2</sub>	33.70	0.85	33.59	0.27	0.12	0.05	0.04	0.10	<0.01	0.22	74.25

(Continued on the following page)

TABLE 2 (Continued) Major elements of the Wujiaping Formation in the region of the eastern Yangtze Block.

Sample	Formation	SiO <sub>2</sub> (%)	Al <sub>2</sub> O <sub>3</sub> (%)	CaO (%)	MgO (%)	K <sub>2</sub> O (%)	Na <sub>2</sub> O (%)	TiO <sub>2</sub> (%)	P <sub>2</sub> O <sub>5</sub> (%)	MnO (%)	Fe <sub>2</sub> O <sub>3</sub> (%)	CIA
JTBP-HF29	P <sub>3</sub> W <sub>2</sub>	88.42	0.64	2.69	0.20	0.18	0.06	0.03	1.09	<0.01	0.39	61.97
JTBP-HF30	P <sub>3</sub> W <sub>2</sub>	13.17	0.18	44.81	2.47	0.02	0.02	0.01	0.02	<0.01	0.02	67.29
JTBP-HF31	P <sub>3</sub> W <sub>2</sub>	19.01	0.19	43.25	0.88	0.03	0.03	<0.01	0.03	<0.01	0.03	59.14

Bioclastic mudstones in the Wujiaping Formation are mainly developed at P<sub>3</sub>W<sub>1</sub>. Macroscopically, bioclastic mudstone is gray, with no obvious bedding. At the micro-scale, plenty of fragments of brachiopods and echinoderms (such as crinoids) can be found in bioclastic mudstone (Figure 2J).

#### 4.1.4 Carbonate rocks

Carbonate rocks in the study area are classified as micrite, calcisphere limestone, bioclastic limestone, bioclastic micrite, and chert nodule and clot limestone.

Micrite in the Wujiaping Formation is mainly distributed in P<sub>3</sub>W<sub>2</sub>. At the macro-scale, the micrite is light gray and gray, and the thickness of a single layer is more than 30 cm. Microscopically, the size of the micrite crystal ranges from 0.01 mm to 0.03 mm (Figure 2K).

Calcsphere limestone is mainly distributed in P<sub>3</sub>W<sub>2</sub>. At the macro-scale, the calcisphere limestone is light gray, and the thickness of a single layer is more than 60 cm. Microscopically, plenty of calcispheres are developed, and the size ranges from approximately 0.12 mm to 0.2 mm (Figure 2L).

Bioclastic limestone is mainly developed in P<sub>3</sub>W<sub>2</sub>. At the macro-scale, the bioclastic limestone is light gray, and the thickness of a single layer is more than 50 cm. At the micro-scale, plenty of bioclasts are developed, such as brachiopods and echinoderms (Figure 2M). The bioclastic limestone in the Wujiaping Formation is mainly developed in the shoal.

Bioclastic micrite is mainly developed in P<sub>3</sub>W<sub>2</sub>. It is mainly composed of micrite, and a few bioclasts, such as brachiopods, can be found (Figure 2N). The bioclastic micrite in the Wujiaping Formation is mainly developed in the restricted platform.

Chert nodules and clot limestone are mainly developed in P<sub>3</sub>W<sub>2</sub>. The chert nodule and clot limestone are light gray, and the thickness of a single layer is more than 80 cm. There is no obvious bedding in it. Plenty of chert nodules and clots can be found, and their size is 4–8 cm and 5–16 cm, respectively (Figure 2O).

## 4.2 Elemental geochemistry

### 4.2.1 CIA

The results of the major element examination and CIA values in the Wujiaping Formation are shown in Table 2.

In well XD-1, the CIA values of P<sub>3</sub>W<sub>1</sub> range from 58.08 to 85.84 (avg. 67.51), and upward, in P<sub>3</sub>W<sub>2</sub>, the CIA values maintain relatively low values, varying between 17.74 and 59.39 (average: 50.27).

The trend of the CIA in the Wujiaping Formation in the JTBP section is similar to that of XD-1. The CIA values of the lower part of P<sub>3</sub>W<sub>1</sub> show a stable range from 63.80 to 79.25 (average: 72.86). In the upper part of P<sub>3</sub>W<sub>1</sub>, the values of the CIA decrease sharply, ranging from 43.57 to 59.90 (average: 49.20).

### 4.2.2 Mo and U

The enrichment factors of Mo and U in the Wujiaping Formation are shown in Table 3.

In well XD-1, the values of both Mo<sub>EF</sub> and U<sub>EF</sub> in the Wujiaping Formation are very low (mainly less than 2), indicating that Mo and U are not enriched during this time. The values of Mo<sub>EF</sub> and

TABLE 3 Trace elements of the Wujiaping Formation in the region of the eastern Yangtze Block.

Sample	Formation	Trace element (ppm)				Redox condition			Hydrodynamic condition
		Mo	U	Zr	Rb	Mo <sub>EF</sub>	U <sub>EF</sub>	Mo <sub>EF</sub> /U <sub>EF</sub>	Zr/Rb
XD-1-HF1	P <sub>3</sub> W <sub>1</sub>	0.34	1.64	489	44.8	0.12	0.40	0.30	10.92
XD-1-HF2	P <sub>3</sub> W <sub>1</sub>	0.76	4.83	1,180	19.8	0.31	1.34	0.23	59.60
XD-1-HF3	P <sub>3</sub> W <sub>1</sub>	2.65	5.74	537	40.9	1.07	1.60	0.67	13.13
XD-1-HF4	P <sub>3</sub> W <sub>1</sub>	2.06	4.11	494	34.7	0.91	1.26	0.73	14.24
XD-1-HF5	P <sub>3</sub> W <sub>1</sub>	1.99	4.76	526	50.4	0.70	1.16	0.61	10.44
XD-1-HF6	P <sub>3</sub> W <sub>1</sub>	2.28	1.93	298	18.0	1.20	0.70	1.71	16.56
XD-1-HF7	P <sub>3</sub> W <sub>1</sub>	2.02	3.48	698	60.2	0.76	0.90	0.84	11.59
XD-1-HF8	P <sub>3</sub> W <sub>1</sub>	1.15	3.57	720	68.2	0.43	0.93	0.47	10.56
XD-1-HF9	P <sub>3</sub> W <sub>1</sub>	1.07	3.94	663	62.8	0.44	1.11	0.39	10.56
XD-1-HF10	P <sub>3</sub> W <sub>1</sub>	0.38	4.28	186	24.5	0.33	2.60	0.13	7.59
XD-1-HF11	P <sub>3</sub> W <sub>2</sub>	1.09	6.60	389	67.9	0.45	1.87	0.24	5.73
XD-1-HF12	P <sub>3</sub> W <sub>2</sub>	0.49	1.13	26.1	2.84	1.86	2.95	0.63	9.19
XD-1-HF13	P <sub>3</sub> W <sub>2</sub>	0.43	1.32	16.5	9.44	1.35	2.85	0.47	1.75
XD-1-HF14	P <sub>3</sub> W <sub>2</sub>	2.65	2.64	28.6	3.68	11.99	8.25	1.45	7.77
XD-1-HF15	P <sub>3</sub> W <sub>2</sub>	0.89	6.06	209	17.3	1.71	8.04	0.21	12.08
XD-1-HF16	P <sub>3</sub> W <sub>2</sub>	0.36	2.04	41.7	3.12	1.22	4.78	0.26	13.37
XD-1-HF17	P <sub>3</sub> W <sub>2</sub>	0.19	0.64	4.30	1.91	22.10	51.40	0.43	2.25
JTBP-HF1	P <sub>3</sub> W <sub>1</sub>	53.4	0.53	0.46	23.2	91.53	0.63	145.92	0.02
JTBP-HF2	P <sub>3</sub> W <sub>1</sub>	45.7	0.12	5.14	164	15.13	0.03	551.55	0.03
JTBP-HF3	P <sub>3</sub> W <sub>1</sub>	87.4	0.36	0.82	58.0	74.12	0.21	351.61	0.01
JTBP-HF4	P <sub>3</sub> W <sub>1</sub>	46.4	0.22	0.51	39.3	48.05	0.16	305.45	0.01
JTBP-HF5	P <sub>3</sub> W <sub>1</sub>	148	0.37	0.48	38.8	155.48	0.27	579.31	0.01
JTBP-HF6	P <sub>3</sub> W <sub>1</sub>	25.7	0.47	0.81	65.1	19.11	0.24	79.19	0.01
JTBP-HF7	P <sub>3</sub> W <sub>1</sub>	53.4	0.55	0.80	59.2	37.24	0.26	140.61	0.01
JTBP-HF8	P <sub>3</sub> W <sub>1</sub>	116	0.76	0.89	67.7	82.13	0.37	221.05	0.01
JTBP-HF9	P <sub>3</sub> W <sub>1</sub>	43.2	0.61	1.06	88.5	24.24	0.24	102.57	0.01
JTBP-HF10	P <sub>3</sub> W <sub>1</sub>	19.7	0.34	0.69	64.9	13.66	0.16	83.91	0.01
JTBP-HF11	P <sub>3</sub> W <sub>1</sub>	13.6	0.14	0.34	25.4	19.60	0.14	140.69	0.01
JTBP-HF12	P <sub>3</sub> W <sub>1</sub>	257	0.50	0.84	72.2	165.41	0.22	744.41	0.01
JTBP-HF13	P <sub>3</sub> W <sub>1</sub>	24.7	0.17	0.15	9.69	86.96	0.41	210.43	0.02

(Continued on the following page)

TABLE 3 (Continued) Trace elements of the Wujiaping Formation in the region of the eastern Yangtze Block.

Sample	Formation	Trace element (ppm)				Redox condition			Hydrodynamic condition
		Mo	U	Zr	Rb	Mo <sub>EF</sub>	U <sub>EF</sub>	Mo <sub>EF</sub> /U <sub>EF</sub>	Zr/Rb
JTBP-HF14	P <sub>3</sub> W <sub>1</sub>	90.3	0.56	0.67	50.5	101.93	0.44	233.53	0.01
JTBP-HF15	P <sub>3</sub> W <sub>1</sub>	334	0.34	0.54	46.2	401.38	0.28	1,422.72	0.01
JTBP-HF16	P <sub>3</sub> W <sub>1</sub>	72.1	0.05	0.12	6.00	479.20	0.22	2131.03	0.02
JTBP-HF17	P <sub>3</sub> W <sub>1</sub>	16.6	0.25	0.37	18.6	25.56	0.27	96.17	0.02
JTBP-HF18	P <sub>3</sub> W <sub>1</sub>	99.5	0.18	0.45	20.3	146.29	0.18	800.57	0.02
JTBP-HF19	P <sub>3</sub> W <sub>2</sub>	112	0.27	0.38	30.6	211.45	0.35	600.77	0.01
JTBP-HF20	P <sub>3</sub> W <sub>2</sub>	12.9	0.07	0.077	10.9	59.59	0.23	259.48	0.01
JTBP-HF21	P <sub>3</sub> W <sub>2</sub>	2.54	0.09	0.084	9.78	12.73	0.31	40.87	0.01
JTBP-HF22	P <sub>3</sub> W <sub>2</sub>	1.62	0.14	0.18	28.2	3.94	0.23	16.76	0.01
JTBP-HF23	P <sub>3</sub> W <sub>2</sub>	2.57	0.09	0.088	14.1	11.87	0.29	40.90	0.01
JTBP-HF24	P <sub>3</sub> W <sub>2</sub>	2.40	0.06	0.078	5.02	18.18	0.29	63.20	0.02
JTBP-HF25	P <sub>3</sub> W <sub>2</sub>	2.08	0.03	0.070	7.15	19.35	0.20	97.17	0.01
JTBP-HF26	P <sub>3</sub> W <sub>2</sub>	2.46	0.05	0.078	7.31	22.89	0.32	71.26	0.01
JTBP-HF27	P <sub>3</sub> W <sub>2</sub>	1.69	0.05	0.068	10.4	11.47	0.21	54.39	0.01
JTBP-HF28	P <sub>3</sub> W <sub>2</sub>	9.62	0.07	0.094	4.86	73.72	0.39	190.85	0.02
JTBP-HF29	P <sub>3</sub> W <sub>2</sub>	6.88	0.12	0.076	4.07	70.02	0.84	83.03	0.02
JTBP-HF30	P <sub>3</sub> W <sub>2</sub>	1.33	0.02	0.040	0.59	48.13	0.40	120.39	0.07
JTBP-HF31	P <sub>3</sub> W <sub>2</sub>	1.47	0.02	0.046	0.95	50.39	0.45	112.05	0.05

U<sub>EF</sub> in P<sub>3</sub>W<sub>1</sub> range from 0.12 to 1.20 (average: 0.63) and 0.40 to 2.60 (average: 1.20) individually. Comparatively speaking, Mo<sub>EF</sub> and U<sub>EF</sub> in P<sub>3</sub>W<sub>2</sub> are higher than in P<sub>3</sub>W<sub>1</sub>, ranging from 0.45 to 22.10 (average: 5.81) and 1.87 to 51.40 (average: 11.45), respectively.

In the JTBP section, the values of Mo<sub>EF</sub> show an opposite trend, especially in P<sub>3</sub>W<sub>1</sub>. In P<sub>3</sub>W<sub>1</sub>, the values of Mo<sub>EF</sub> were between 15.13 and 479.21 (avg. 110.39), while in P<sub>3</sub>W<sub>2</sub>, the average value of Mo<sub>EF</sub> decreased to 47.21 (from 3.94 to 211.45). Although the values of U<sub>EF</sub> were all less than 1 in the whole Wujiaping Formation, the ratio of Mo<sub>EF</sub>/U<sub>EF</sub> values ranged from 79.19 to 2131.03 (average: 463.37) in P<sub>3</sub>W<sub>1</sub> and 16.76 to 600.77 (average: 134.7) in P<sub>3</sub>W<sub>2</sub>, respectively.

#### 4.2.3 Zr/Rb

The values of Zr/Rb ratios in the Wujiaping Formation are shown in Table 3.

In well XD-1, the Zr/Rb ratios of P<sub>3</sub>W<sub>1</sub> range from 10.56 to 59.60 (average: 17.51). Upward, the values of Zr/Rb ratios decrease to 7.47 (from 1.75 to 13.37) in P<sub>3</sub>W<sub>2</sub>.

In the JTBP section, the values of Zr/Rb ratios of the Wujiaping Formation vary from 0.01 to 0.07 (average: 0.02).

## 5 Discussion

### 5.1 Significance of the development of bauxite

Based on the differences in genesis, bauxite can be divided into sedimentary bauxite, accumulation bauxite, laterite bauxite, and magmatic bauxite (Liu et al., 2002; Liu et al., 2022; Gao et al., 2014).

The bauxite in the study area is mainly developed at the bottom of the Wujiaping Formation, and its formation may be related to the Dongwu movement. Because of the Dongwu movement, the carbonate rocks in the Maokou Formation were exposed to the earth's surface and encountered weathering and denudation, and a paleo-crust of weathering was formed. In the sedimentary period of the Wujiaping Formation, the bauxite was formed autochthonously or transported nearby.

The bauxite in the WJP Formation is more likely to be sedimentary bauxite, and the distribution of the bauxite may also be the scope of the paleo-uplift. The observation of thin

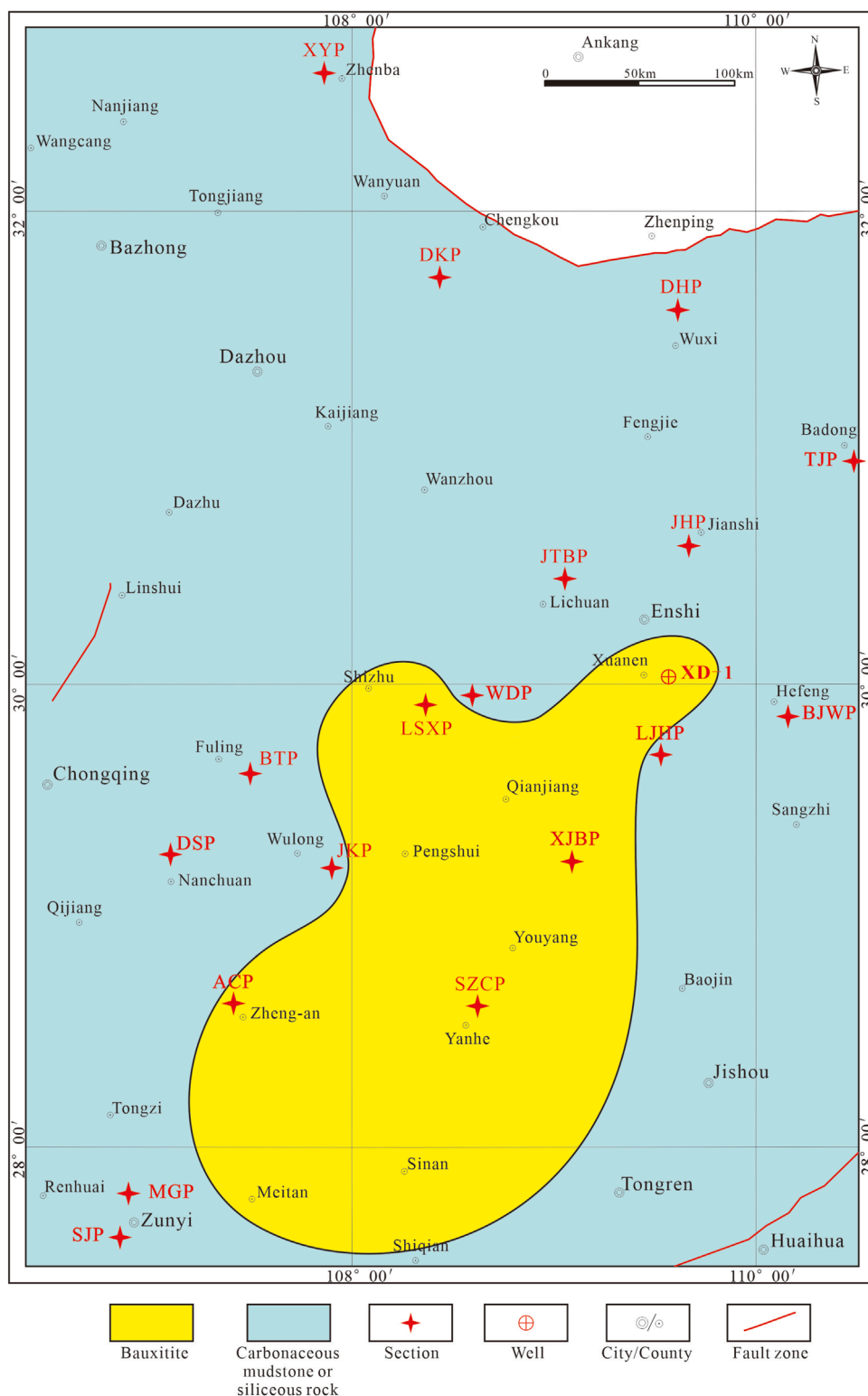
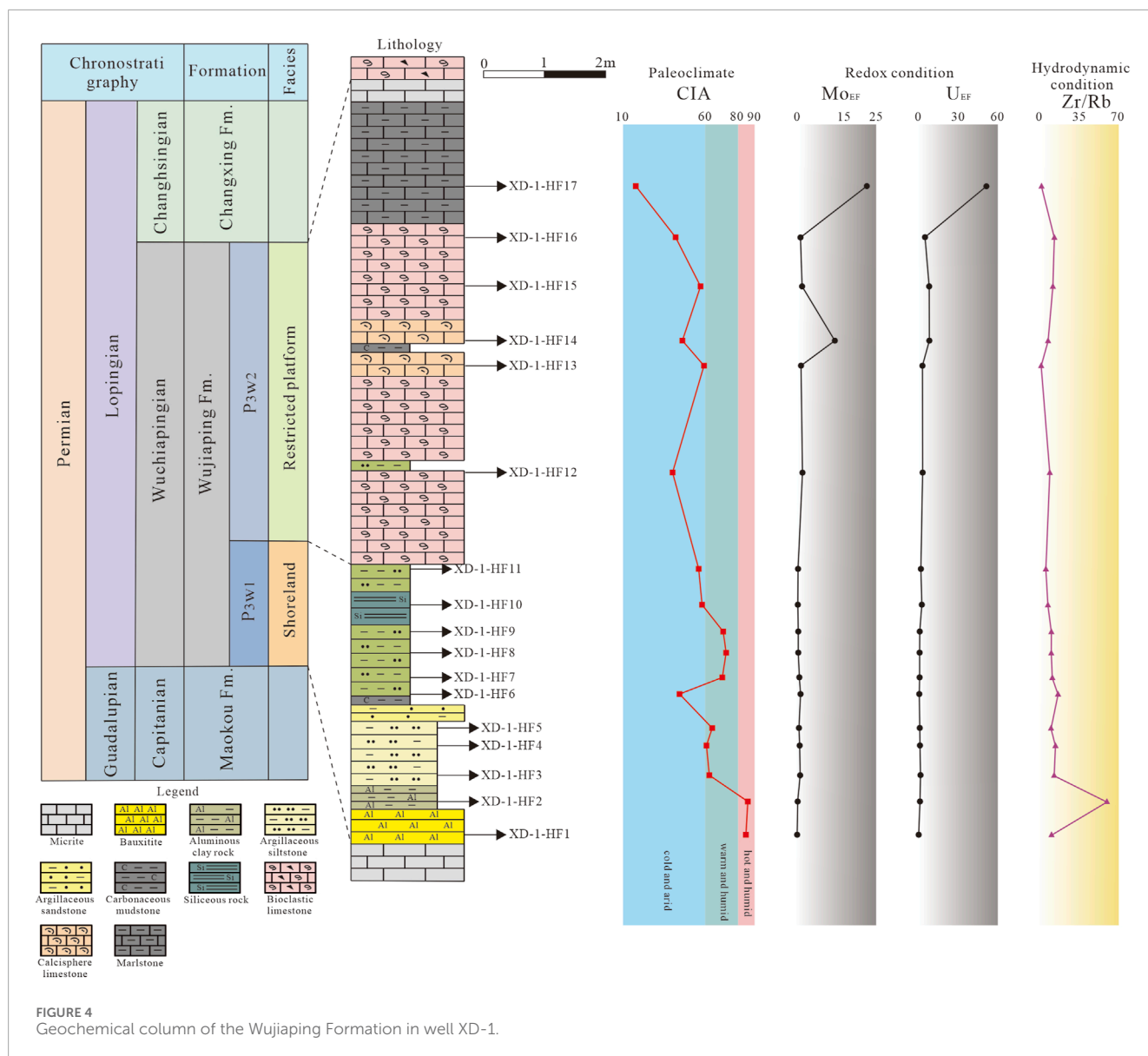


FIGURE 3 Distribution of bauxite at the bottom of the Wujiaping Formation in the study area.

sections showed that the bauxite of the Wujiaping Formation is developed in the area of Shizhu-Sinan-Xuanen, which is also the range of the paleo-uplift before the sedimentary of the WJP Formation (Figure 3).

### 5.2 Paleoclimate

The CIA values show that the paleoclimate of the bottom of the Wujiaping Formation in well XD-1 was hot and humid, which is



consistent with the formation of the paleo-crust of weathering. The hot and humid climate would favor the weathering and denudation of carbonate rocks in the Maokou Formation. Upward, it underwent two circulations of warm–humid and cold–arid in P<sub>3</sub>W<sub>1</sub>. In P<sub>3</sub>W<sub>2</sub>, the paleoclimate was cold and arid persistently. The fluctuations in the CIA value show that well XD-1 underwent the hot–warm–cold process in the Wujiaping Formation (Figure 4).

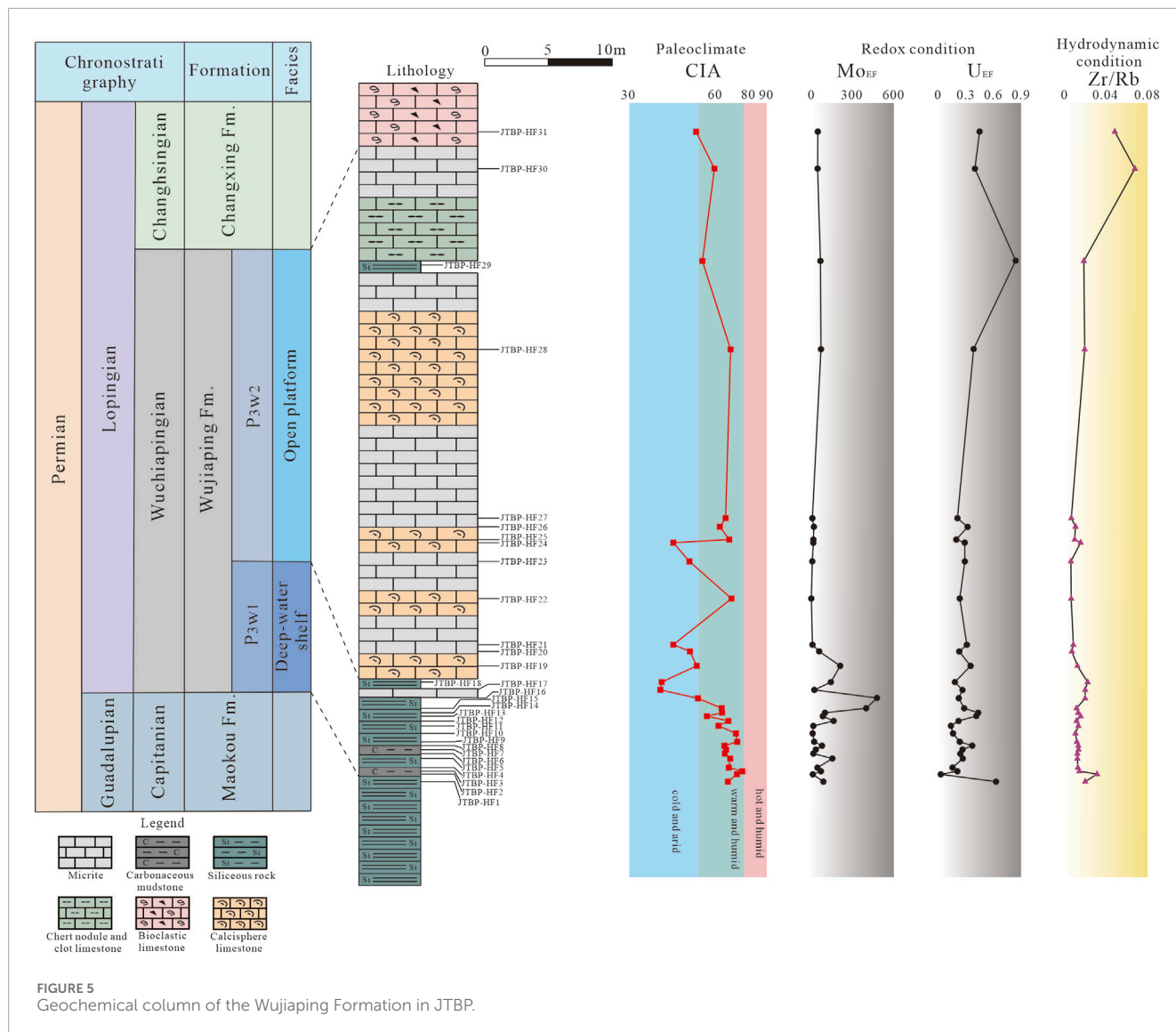
In the JTBP section, the values of the CIA show that the paleoclimate of P<sub>3</sub>W<sub>1</sub> changes from warm–humid to cold–arid. In the lower part of P<sub>3</sub>W<sub>2</sub>, the paleoclimate stayed cold and arid, while in the upper part of P<sub>3</sub>W<sub>2</sub>, the paleoclimate converted into warm and humid. At the end of P<sub>3</sub>W<sub>2</sub>, the climate became cold and arid again. The fluctuations in the CIA value show that the JTBP section has experienced the warm and humid–cold and arid–warm and humid process in the Wujiaping Formation (Figure 5).

In general, the paleoclimate during the Wuchiapingian Stage changes from warm and humid in P<sub>3</sub>W<sub>1</sub> to cold and arid in P<sub>3</sub>W<sub>2</sub>.

### 5.3 Redox conditions

In well XD-1, the values of both Mo<sub>EF</sub> and U<sub>EF</sub> in the Wujiaping Formation are mostly less than 2, and the Mo<sub>EF</sub> and U<sub>EF</sub> values in P<sub>3</sub>W<sub>2</sub> are higher than those in P<sub>3</sub>W<sub>1</sub>. It indicates that the reductibility of seawater in P<sub>3</sub>W<sub>2</sub> was stronger than that in P<sub>3</sub>W<sub>1</sub> although the water redox conditions in both P<sub>3</sub>W<sub>1</sub> and P<sub>3</sub>W<sub>2</sub> were oxidic. The ratio of Mo<sub>EF</sub>/U<sub>EF</sub> ranges from 0.23 to 1.71 (avg. 0.58), which shows the same redox condition as the Mo<sub>EF</sub> and U<sub>EF</sub> (Figure 4).

In the JTBP section, the values of Mo<sub>EF</sub> show an opposite trend, especially in P<sub>3</sub>W<sub>1</sub>. In P<sub>3</sub>W<sub>1</sub>, the values of Mo<sub>EF</sub> show strong reductibility of seawater, while in P<sub>3</sub>W<sub>2</sub>, the average value of Mo<sub>EF</sub> decreased, indicating weaker reductibility than the former. The values of U<sub>EF</sub> were all less than 1, but the ratio of Mo<sub>EF</sub>/U<sub>EF</sub> in P<sub>3</sub>W<sub>1</sub> is much larger than that in P<sub>3</sub>W<sub>2</sub>, which also shows the stronger reductibility of P<sub>3</sub>W<sub>1</sub> than P<sub>3</sub>W<sub>2</sub>. Therefore, it is obvious that the water redox conditions of the whole Wujiaping Formation in the



JTBP section are anoxic, and the reductibility in P<sub>3</sub>W<sub>2</sub> is weaker than in P<sub>3</sub>W<sub>1</sub> (Figure 5).

### 5.4 Hydrodynamic conditions

In well XD-1, the Zr/Rb ratios in P<sub>3</sub>W<sub>1</sub> decrease more rapidly than in P<sub>3</sub>W<sub>2</sub>. It shows that the seawater hydrodynamic condition in P<sub>3</sub>W<sub>1</sub> was stronger than in P<sub>3</sub>W<sub>2</sub> (Figure 4).

For the JTBP section, the values of Zr/Rb ratios of the whole Wujiaping Formation are very low, which indicates that the seawater hydrodynamic condition in the JTBP section was weak, consistent with the anoxic environment from the analysis above (Figure 5).

### 5.5 Sedimentary facies

Through the observation of the thin sections and the analysis of the geochemical data, the sedimentary

facies of the Wujiaping Formation in the study area are classified into shoreland, shallow-water shelf, deep-water shelf, and shoal.

#### 5.5.1 Shoreland

Because of the Dongwu Movement, the carbonate rocks in the Maokou Formation were unevenly lifted and encountered weathering and denudation, forming the paleo-weathering crust (Figure 2A). Bauxite is developed at the bottom of the WJP Formation in well XD-1 and LSXP in the paleo-weathering crust. Overlying the bauxite, argillaceous siltstones with few parallel and cross-beddings are also observed (Figure 2F), which shows the high hydrodynamic conditions in these two areas. Combined with the inheritance of the paleo-topography affected by the Dongwu Movement, we believe that shoreland is developed in the study area. In addition, based on the geochemical analysis in well XD-1, the redox conditions are oxic, and its values of Zr/Rb show high hydrodynamic conditions, which are also in agreement with the development of shoreland (Figure 4).

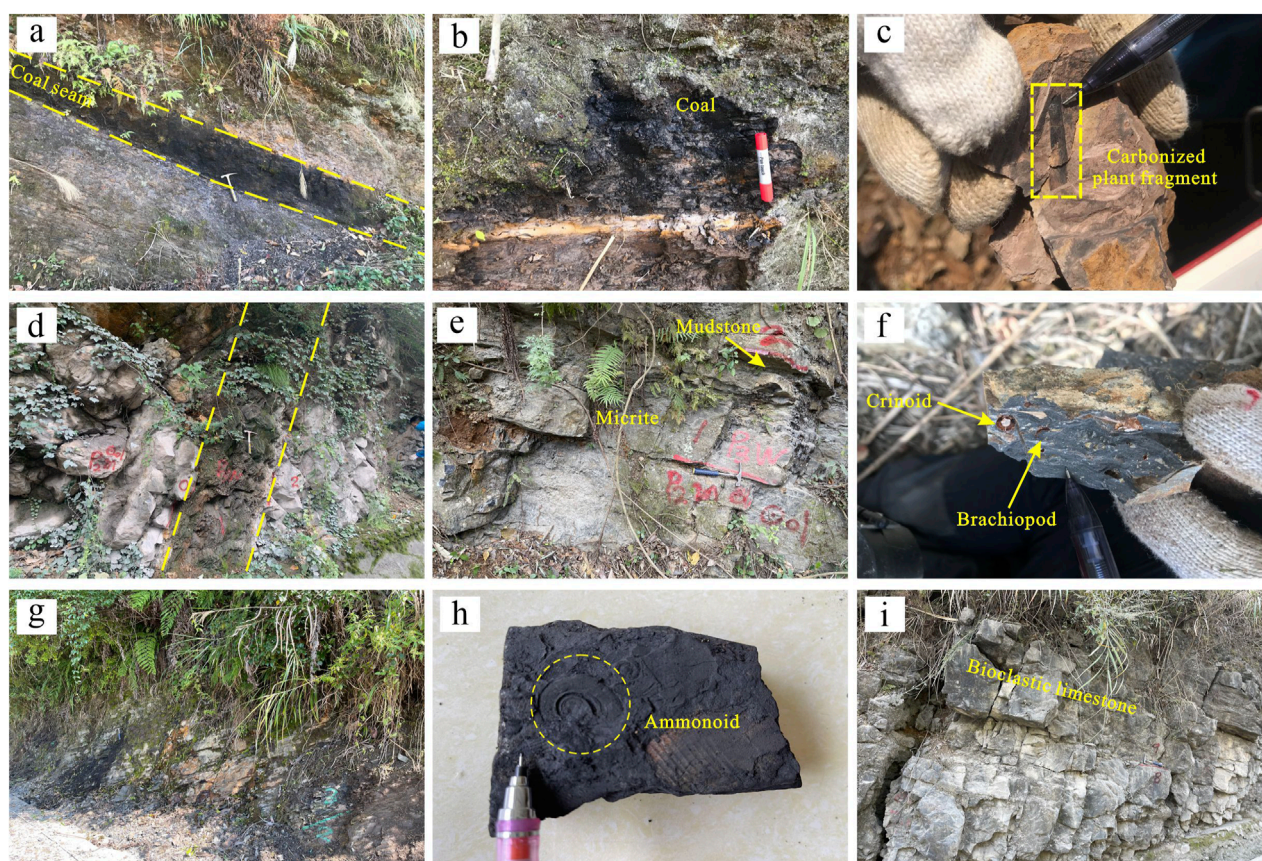


FIGURE 6

Macroscopic characteristics of different sedimentary facies in the Wujiaping Formation in the eastern Yangtze Block. (A) Coal seam,  $P_3W_1$ , MGP; (B) Enlargement for (A),  $P_3W_1$ , MGP; (C) carbonized plant fragments,  $P_3W_1$ , SJP; (D) mudstone and carbonaceous mudstone,  $P_3W_1$ , BTP; (E) micrite, interlayered with mudstone,  $P_3W_1$ , JKP; (F) crinoid and brachiopod in bioclastic limestone,  $P_3W_1$ , XJBP; (G) siliceous rock,  $P_3W_1$ , JTBP; (H) ammonoid in siliceous mudstone,  $P_3W_1$ , JTBP; and (I) heavy-layer bioclastic limestone,  $P_3W_2$ , JKP.

In the MGP, a coal seam with a thickness of 43 cm and an interlayer of carbonaceous mudstone is developed in lower  $P_3W_1$  (Figures 6A,B). Furthermore, in the carbonaceous mudstone of the SJP, carbonized plant fragments are observed in  $P_3W_1$  (Figure 6C). Therefore, the marsh was undoubtedly developed in shoreland.

### 5.5.2 Shallow-water shelf

The shallow-water shelf is the shallow-water area between the storm wave base and the normal wave base, the depth of which mainly ranges from 10 m to 200 m.

In the study area, the shallow-water shelf was mainly developed in the lower WJP Formation. In BTP, the lithology at the lower WJP Formation is characterized by mudstone and argillaceous siltstone, and we prefer the shoreland of the sedimentary environment (Figure 6D). Adjacent to BTP, micrite is observed in JKP (Figure 6E), which indicates the different sedimentary facies between them. In addition, in the same strata of the WJP Formation in SZCP and XJBP, bioclastic micrite is observed, with a few brachiopods and crinoids in it (Figure 6F). There must be sedimentary facies that are mainly composed of carbonate rocks and located on the seaward side of the shoreland, that is, shallow-water shelf. In addition to the

carbonate rocks, clastic rocks, such as mudstone, are also observed as the interlayer between carbonates in the JKP (Figure 6E).

### 5.5.3 Deep-water shelf

The deep-water shelf refers to the area below the storm wave base, where wave action is weaker than that in the shallow-water shelf.

In JTBP, 3.6-m-thick siliceous rock and siliceous mudstone, interlayered with carbonaceous mudstone, are found at the bottom of the WJP Formation, which shows significant differences from the sediments in JKP and XJBP (Figure 6G). In the siliceous mudstone, few ammonoids are recognized (Figure 6H). In addition, the geochemical analysis shows the strong reductibility of redox conditions in JTBP, compared with both the overlying strata in the JTBP and the same strata in well XD-1 (Figure 4). The sedimentary facies in the JTBP are more likely to be the deep-water shelf.

### 5.5.4 Restricted platform

During the sedimentary period of  $P_3W_2$ , further east of the study area, grainstone with sparry calcite cementation and breccia limestone are found, and the thickness can be more than 300 m (Zhao et al., 2012). It indicates that the rimmed



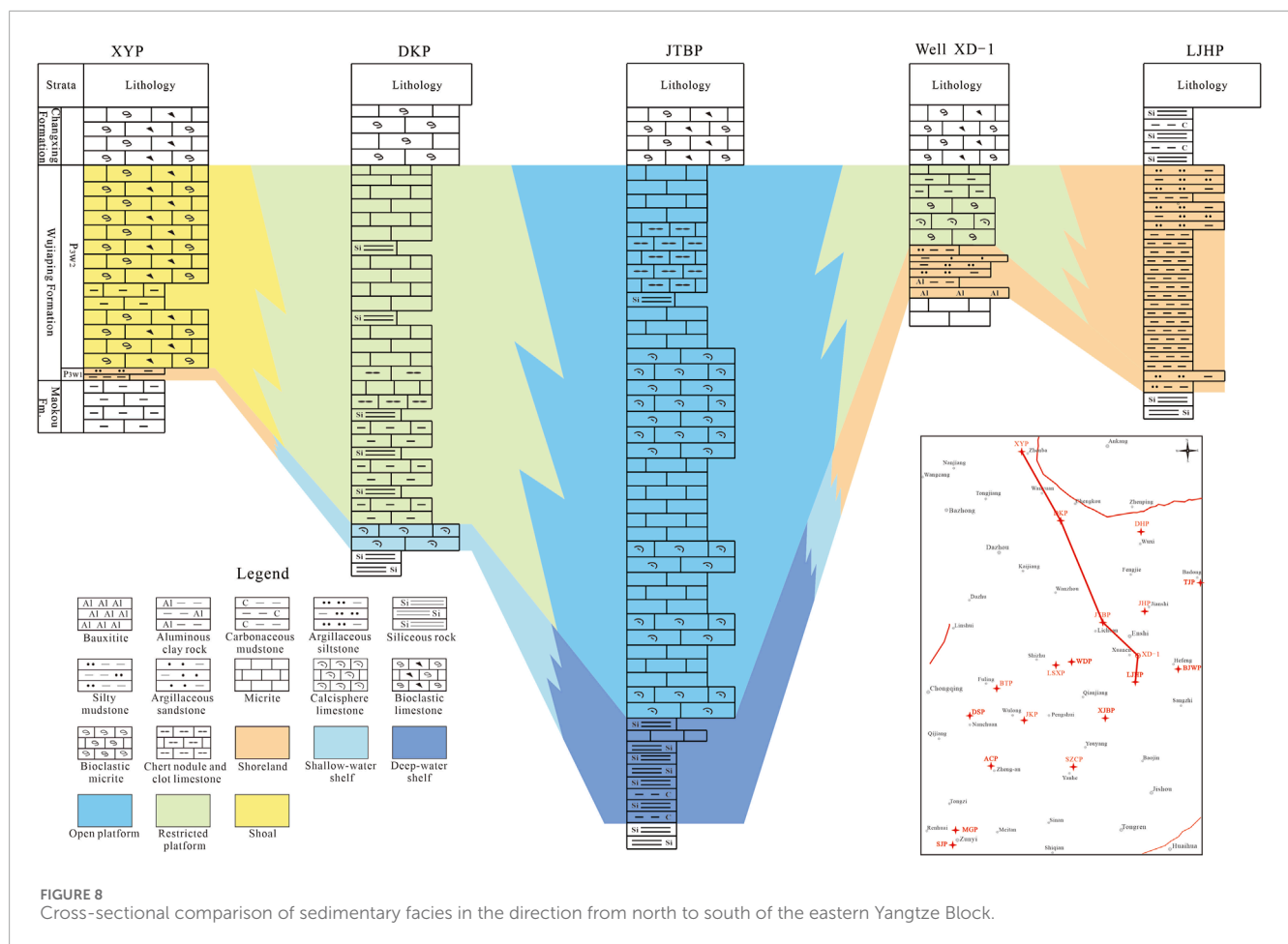


**FIGURE 8** Cross-sectional comparison of sedimentary facies in the direction from north to south of the eastern Yangtze Block.

In the comparison chart of sedimentary facies from west to east, during the sedimentary period of P<sub>3</sub>W<sub>1</sub>, shoreland, shallow-water shelf, deep-water shelf, shallow-water shelf, and shoreland are developed eastward in turn. In P<sub>3</sub>W<sub>2</sub>, the sedimentary facies are dominated by the restricted platform and open platform, and few patched shoals can be found in BTP (Figure 7).

In the comparison chart of sedimentary facies from north to south, in P<sub>3</sub>W<sub>1</sub>, shoreland, shallow-water shelf, deep-water shelf and shoreland are identified in turn. In P<sub>3</sub>W<sub>2</sub>, the restricted platform, open platform, and patched shoals can also be found, while in LJHP, shoreland is still developed in the upper WJP Formation (Figure 8).

Based on the analysis of the sedimentary facies, during the sedimentary period of P<sub>3</sub>W<sub>1</sub>, slow transgression occurred in the Early Wuchiapingian. Most of the study area is mainly composed of clastic rock, formed in the sedimentary environment of shoreland (Figure 9). The lithologies are mainly composed of bauxite, argillaceous siltstones, carbonaceous mudstone, bioclastic mudstone, and argillaceous mudstone. In the areas of Wulong, Yanhe, and Nanjiang, shallow-water shelves are developed with the lithology of micrite and bioclastic limestone. In the Wuxi and Lichuan areas, deep-water shelf is recognized. Black siliceous rocks were mainly deposited in the deep-water shelf, and complete ammonite fossils were also found. On the whole, during the sedimentary period of P<sub>3</sub>W<sub>1</sub> in the study area, the seawater was the deepest in the Wuxi–Lichuan area, indicating that during the Dongwu Movement, the Wuxi–Lichuan area may have formed a

tectonic depression with the reductive sedimentary environment, which is conducive to the deposition of organic-rich shale.

In P<sub>3</sub>W<sub>2</sub>, carbonates gradually replaced clastic rocks after a short period of mixed deposition of clastic rocks and carbonate rocks, and the main sedimentary facies changed to the restricted platform and open platform, showing a gradual deepening trend from east to west. In the restricted platform, there are three patched shoals in the areas of Fuling–Wulong, Yanhe, and Zhenba, while in the west and southeast of the study area, shoreland is still developed, which is mainly composed of carbonaceous mudstone, partially composed of argillaceous siltstone, and a small amount of siliceous rock (Figure 10).

### 5.7 Sedimentary evolution

Based on the literature research and comprehensive analysis of rock types, sedimentary facies, and geochemical analysis of the Wujiaoping Formation in the study area, the sedimentary evolution model from the Middle Permian Maokou Formation to the Upper Permian Changxing Formation is shown in Figure 11.

During the period of P<sub>2</sub>m, a restricted platform, shallow-water shelf, and deep-water basin were developed in the study area. Some patched shoals can also be found on restricted platforms. Because of the Dongwu Movement, carbonates of the Maokou Formation were exposed to the surface and encountered strong weathering.

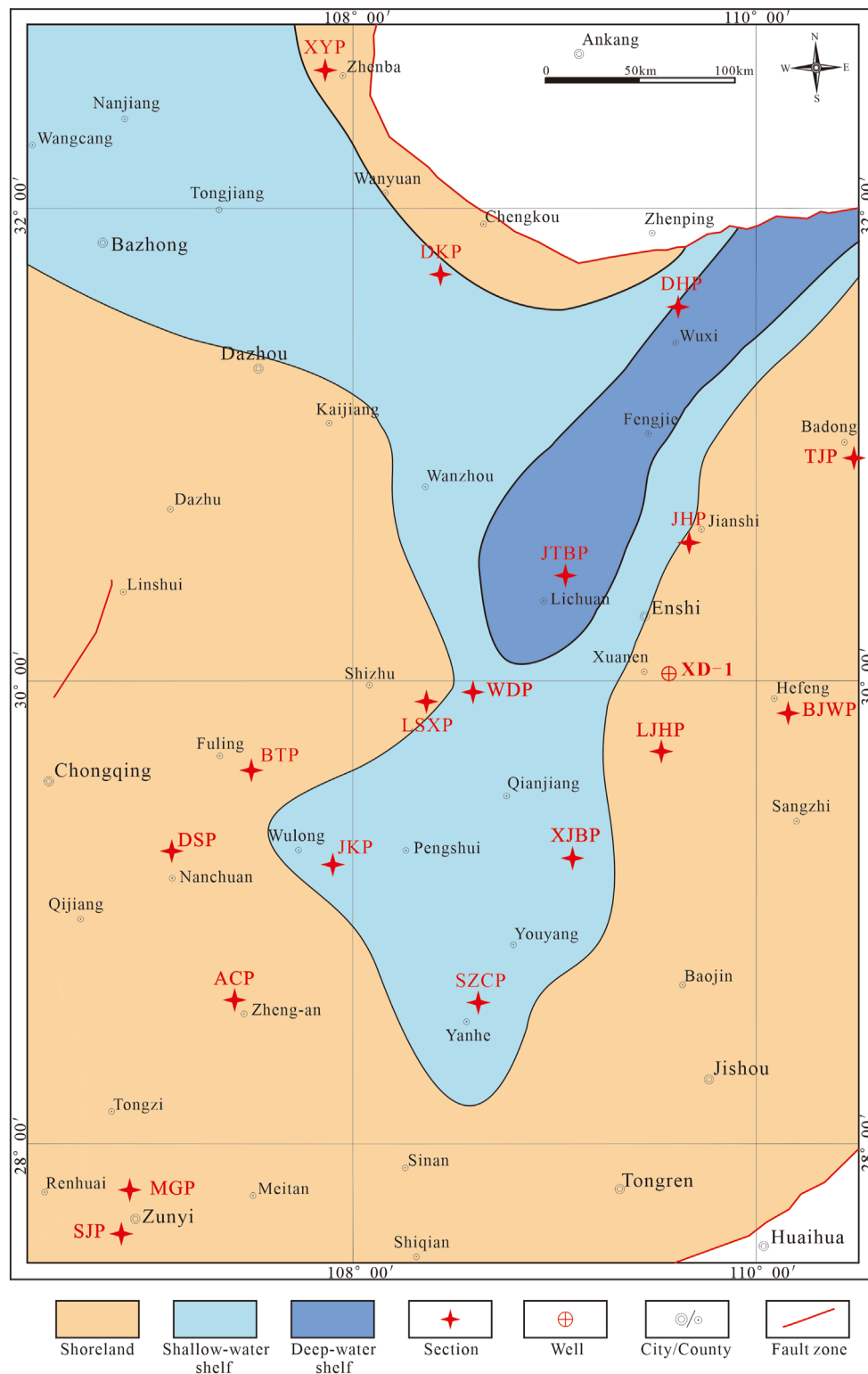
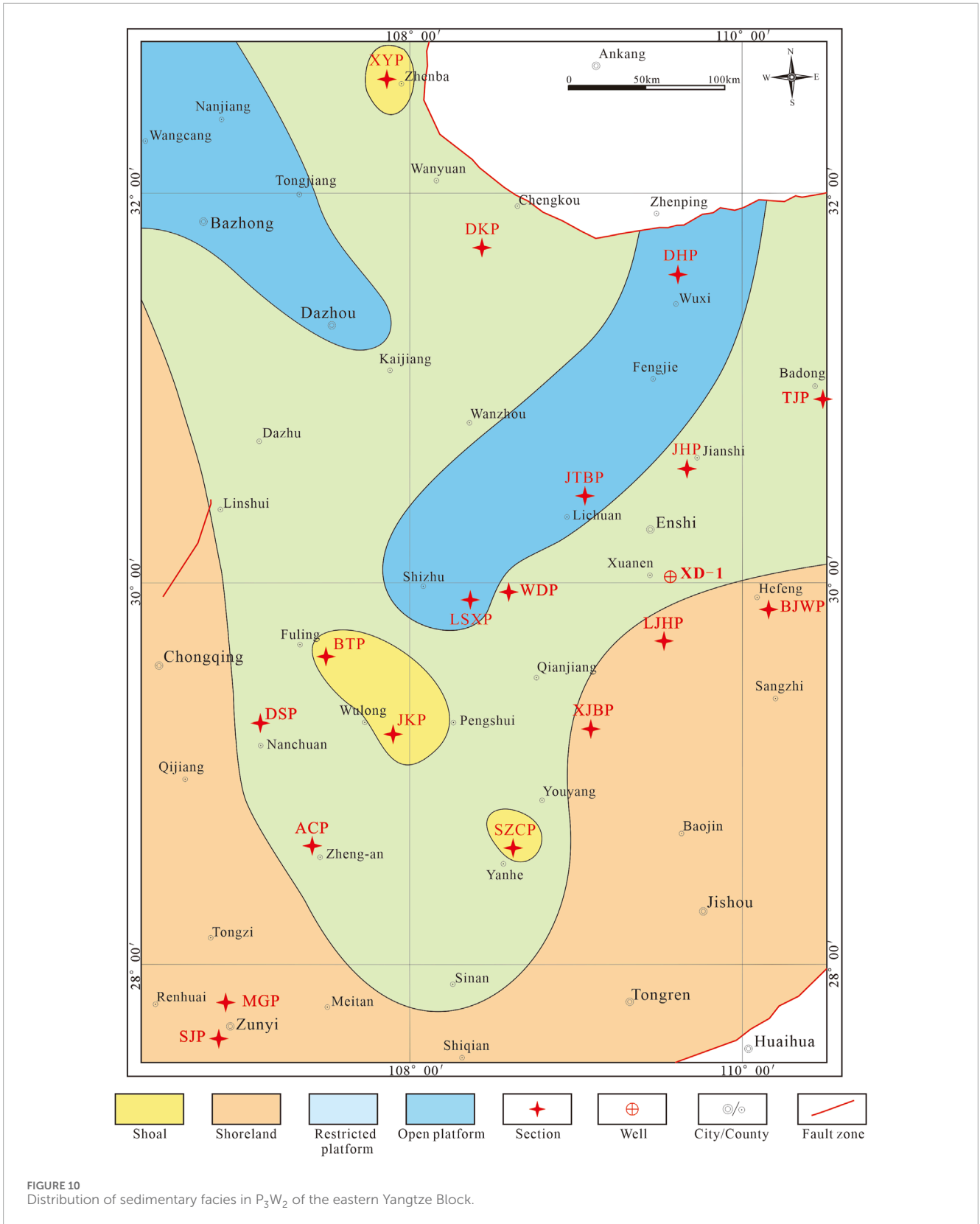


FIGURE 9 Distribution of sedimentary facies in  $P_3W_1$  of the eastern Yangtze Block.

Therefore, bauxite was developed in some areas, and shoreland can also be found around the paleo-uplift.

In the period of  $P_3W_1$ , shoreland, shallow-water shelf, and deep-water shelf were developed in the study area, which was related to the transgression.

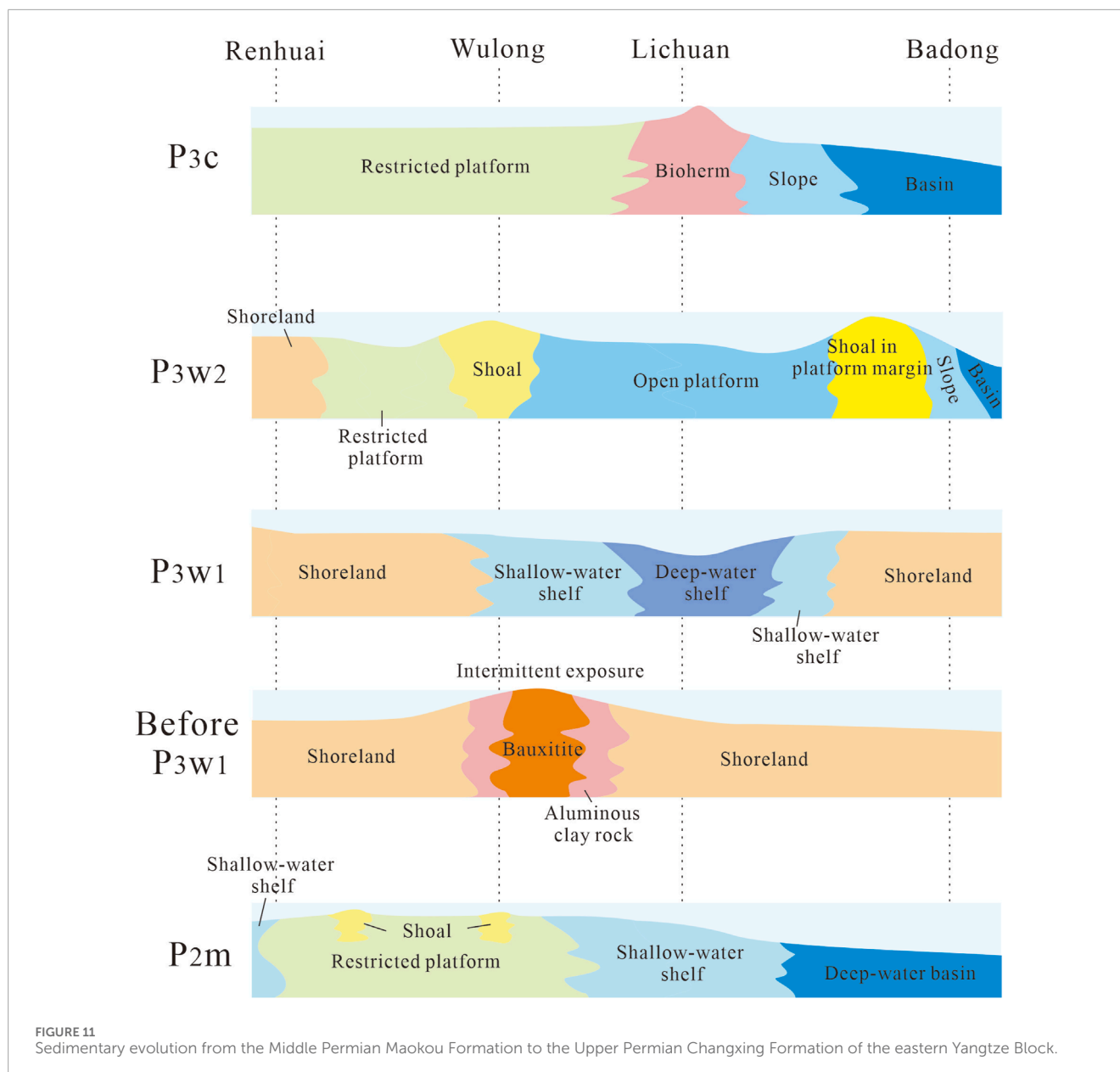
During the period of  $P_3W_2$ , a rimmed carbonate platform was formed. The restricted platform and open platform are developed. A few patched shoals can be found in Fuling–Wulong, Yanhe, and Zhenba. A shoreland was still present in the eastern Sichuan Basin.



In the period of  $P_3c$ , the restricted platform, bioherm, slope, and basin were developed from west to east.

To sum up, the carbonate platform was mainly developed in the sedimentary period of the Maokou Formation. Because of the

Dongwu Movement, most of the study area was uplifted and exposed to the surface. The carbonate platform was partially destroyed with the deposition of clastic sediments and the presence of mixed sedimentation. During the period of  $P_3W_2$ , a carbonate platform was



formed again because of the transgression. In the period of P<sub>3c</sub>, a typical rimmed carbonate platform was finally formed.

## 6 Conclusion

In the study area, 11 rock types are classified in the Wujiaping Formation, including bauxite, siliceous clastic rocks (siliceous rocks and argillaceous siltstone), mudstone (carbonaceous mudstone, siliceous mudstone, and bioclastic mudstone), and 4 types of carbonates (micrite, calcisphere limestone, bioclastic limestone, bioclastic micrite, and chert nodule and clot limestone).

Due to the Dongwu Movement, the carbonate rocks of the Maokou Formation were exposed to the surface, encountering strong weathering and denudation, which formed the

paleo-weathering crust. During the Early Wuchiapingian, slow transgression occurred in the study area. Bauxite and argillaceous siltstone were deposited in shoreland, while carbonaceous mudstone and coal seams formed in the marsh, micrite in the shallow-water shelf, and siliceous rock in the deep-water shelf. During this time, the carbonate platform in the Maokou Formation was partially destroyed, resulting in mixed sedimentation of clastic rocks and carbonate rocks. In the Late Wuchiapingian, a rimmed carbonated platform started to form in the study area, with the restricted platform, open platform, and patched shoals.

From the analysis of lithology and sedimentary facies, a large amount of carbonaceous mudstone and siliceous rocks were widely developed in the Early Wuchiapingian, which shows the substantial potential of source rock for future gas and oil exploration.

## Data availability statement

The original contributions presented in the study are included in the article/Supplementary Material; further inquiries can be directed to the corresponding author.

## Author contributions

YW: funding acquisition, writing—original draft, and writing—review and editing. HL: funding acquisition, supervision, and writing—review and editing. CM: conceptualization, supervision, and writing—review and editing. WC: data curation, visualization, and writing—review and editing. CG: data curation, visualization, and writing—review and editing. WL: investigation, methodology, and writing—review and editing. BZ: data curation, investigation, methodology, and writing—review and editing. QH: data curation, investigation, visualization, and writing—review and editing. YX: data curation, investigation, visualization, and writing—review and editing.

## Funding

The author(s) declare that financial support was received for the research, authorship, and/or publication of this article. Financial support for the research was provided by the Project of SINOPEC Science and Technology Department (Strategic Selection and Evaluation of Mineral Rights in Sichuan Basin and its Periphery, P21086-2, Special Subject 8: Research and Application of Evaluation Technology of Strategic Constituency in Sichuan Basin and its Periphery), the Open Funds of the Key Laboratory of Sedimentary Basins and Petroleum Resources of the Ministry of Natural Resources (cdcgs2022005 and cdcgs2023002), the Chongqing Natural Science Foundation (2024NSCQ-MSX0819), the Science

## References

- Algeo, T. J., and Tribouillard, N. (2009). Environmental analysis of paleoceanographic systems based on molybdenum-uranium covariation. *Chem. Geol.* 268, 211–225. doi:10.1016/j.chemgeo.2009.09.001
- Brumsack, H. J. (2006). The trace metal content of recent organic carbon-rich sediments: implications for Cretaceous black shale formation. *Palaeogeogr. Palaeoclimatol. Palaeoecol.* 232, 344–361. doi:10.1016/j.palaeo.2005.05.011
- Cai, J. (2017). Characteristics of shale gas accumulation in the Wujiaping Formation of the western Hubei and eastern Chongqing. *Petroleum Geol. Eng.* 31, 13–16. doi:10.3969/j.issn.1673-8217.2017.02.004
- Cao, T. T., Deng, M., Liu, G. X., Cao, Q. G., Liu, H., and Huang, Y. R. (2018). Reservoir characteristics of organic-rich siliceous shale of permian Wujiaping Formation in lichuan area, western hubei province. *Mar. Orig. Pet. Geol.* 23, 32–42. doi:10.3969/j.issn.1672-9854.2018.03.004
- Chai, F. Y. (2019). Study on Paleozoic sedimentary facies and favorable area evaluation in Lower Yangtze Basin. *Reserv. Eval. Dev.* 9, 7–12.
- Fan, Y. F. (2016). *Interrelationship between tectonism and hydrocarbon accumulation in marine strata at critical tectonic moment in west Hubei-east Chongqing, South China*. Wuhan, China: Ph. D. Thesis, China University of Geosciences, 145.
- Fedo, C. M., Nesbitt, H. W., and Young, G. M. (1995). Unraveling the effects of K metasomatism in sedimentary rocks and paleosols with implications for palaeoweathering conditions and provenance. *Geology* 23, 921–924. doi:10.1130/0091-7613(1995)0232.3.CO;2
- Fu, X. G., Wang, J., Chen, W. B., Feng, X. L., Wang, D., Song, C. Y., et al. (2015). Organic accumulation in lacustrine rift basin: constraints from mineralogical and

and Technology Research Project of Chongqing Municipal Education Commission (KJQN202201411 and KJQN202301410), the Key Projects of Technological Innovation and Application Development in Chongqing (CSTB2022TIAD-KPX0196), the Chongqing Talent Innovation and Entrepreneurship Team Project (CQYC202203091274), and the Cooperative Projects between Undergraduate Universities in Chongqing and Institute Affiliated with the Chinese Academy of Sciences (HZ2021014).

## Acknowledgments

The authors acknowledge the Sinopec Science and Technology Department, Ministry of Natural Resources, Chongqing Municipal Education Commission, Chongqing Natural Science Foundation, and Chengdu Center of China Geological Survey.

## Conflict of interest

Author HL was employed by SINOPEC.

The remaining authors declare that the research was conducted in the absence of any commercial or financial relationships that could be construed as a potential conflict of interest.

## Publisher's note

All claims expressed in this article are solely those of the authors and do not necessarily represent those of their affiliated organizations, or those of the publisher, the editors, and the reviewers. Any product that may be evaluated in this article, or claim that may be made by its manufacturer, is not guaranteed or endorsed by the publisher.

multiple geochemical proxies. *Int. J. Earth Sci.* 104, 495–511. doi:10.1007/s00531-014-1089-3

Gao, L., Wang, D. H., Xiong, X. Y., and Yi, C. W. (2014). Summary on aluminum ore deposits minerogenetic regulation in China. *Acta Geol. Sin.* 88, 2284–2295. doi:10.3969/j.issn.0001-5717.2014.12.010

Gu, Z. X., Peng, Y. M., He, Y. B., Hu, Z. Q., and Zhai, Y. J. (2015). Geological conditions of Permian sea-land transitional facies shale gas in the Xiangzhong Depression. *Geol. China* 42, 288–299.

Hu, Y., Li, H., Zeng, H. S., Yuan, X. Y., and Song, X. B. (2020). Natural gas genesis diversity of Chishui in the southern Sichuan. *Special oil and Gas Reserv.* 27, 51–56.

Jiang, Y. Q., Diao, Z. L., Xu, C. H., Feng, L., Gu, Y. F., and Yi, J. Z. (2019). Characteristics and controlling factors of Permian reef beach reservoir in platform-depression margin of eastern Sichuan Basin. *Special oil and Gas Reserv.* 27, 7–13. doi:10.3969/j.issn.1006-6535.2020.05.002

Li, G. L., Wang, X. H., Bai, D. Y., Luo, P., and Jiang, W. (2015a). Potentiality exploration of the upper permian longtan formation shale gas in central and southeastern human province. *Geol. Sci. Technol. Inf.* 34, 133–138.

Li, J., Yu, B. S., Xia, X. H., Tian, Y. K., Li, Y. L., Zhou, H., et al. (2015b). The characteristics of the Upper Permian shale reservoir in the northwest of Guizhou Province, China. *Earth Sci. Front.* 22, 301–311. doi:10.13745/j.esf.2015.01.026

Liang, D. G., Guo, T. L., Chen, J. P., Bian, L. Z., and Zhao, Z. (2008). Distribution of four suits of regional marine source rocks. *Mar. Orig. Pet. Geol.* 13, 1–16. doi:10.3969/j.issn.1672-9854.2008.02.001

- Liang, X. W., and Li, L. (2021). Geological conditions and exploration potential for shale gas in Upper Permian Wujiaping Formation in the region of western Hubei-eastern Chongqing. *Petroleum Geol. and Exp.* 43, 386–393. doi:10.11781/sydz202103386
- Lin, L. B., Chen, H. D., and Zhu, L. D. (2009). Sequence-based lithofacies and paleogeographic characteristics of Wujiaping Formation, eastern Sichuan Basin. *Petroleum Geol. Recovery Effic.* 16, 42–45. doi:10.3969/j.issn.1009-9603.2009.06.011
- Liu, G. X., Jin, Z. J., Deng, M., Zhai, C. B., Guan, H. L., and Zhang, C. J. (2015). Exploration potential for shale gas in the upper permian longtan Formation in eastern Sichuan Basin. *Oil and Gas Geol.* 36, 481–487. doi:10.11743/ogg20150317
- Liu, K. K., Fu, X., Rong, W., Wan, J. Q., Lin, J., and Jiang, Y. P. (2022). Analysis of bauxite reservoir in xarea of ordos basin. *J. Xi'an Shiyou Univ. Nat. Sci. Ed.* 37, 25–31. doi:10.3969/j.issn.1673-064X.2022.02.004
- Liu, X. T., Ma, Z. X., and Yan, J. X. (2010). Sedimentary environments and controlling factors of hydrocarbon source rocks of the Late Permian Wujiaping age in Yangtze area. *J. Palaeogeogr.* 12, 244–252. doi:10.7605/gdxb.2010.02.012
- Liu, Z. S., Zhao, H. T., Fan, S. Q., and Chen, S. Q. (2002). *Geology of the south China sea*. Beijing, China: Beijing Science Press, 502.
- Luo, J. X., and He, Y. B. (2014). *Lithofacies palaeogeography of the permian in middle and upper Yangtze region*. Beijing: Petroleum Industry Press, 202.
- Ma, P. F., Wang, L. C., Wang, C. S., Wu, X. H., and Wei, Y. S. (2015). Organic-matter accumulation of the lacustrine lunpola oil shale, central Tibetan plateau: controlled by the paleoclimate, provenance, and drainage system. *Int. J. Coal Geol.* 147–148, 58–70. doi:10.1016/j.coal.2015.06.011
- McLennan, S. M. (1993). Weathering and global denudation. *J. Geol.* 101, 295–303. doi:10.1086/648222
- Nesbitt, H. W., and Young, G. M. (1982). Early Proterozoic climates and plate motions inferred from major element chemistry of lutites. *Nature* 299, 715–717. doi:10.1038/299715a0
- Ross, D. J. K., and Bustin, R. M. (2009). Investigating the use of sedimentary geochemical proxies for paleoenvironment interpretation of thermally mature organic-rich strata: examples from the Devonian-Mississippian shales, Western Canadian Sedimentary Basin. *Chem. Geol.* 260, 1–19. doi:10.1016/j.chemgeo.2008.10.027
- Teng, G. E., Qian, J. Z., Fu, X. D., Yang, Y. F., and Xie, X. M. (2010). Hydrocarbon source rocks evaluation of the upper permian Wujiaping Formation in northeastern sichuan area. *J. Palaeogeogr.* 12, 334–345. doi:10.1145/1836845.1836984
- Tian, Y., Zhang, X. Y., He, Y. B., Luo, J. X., Zhou, H., Zhou, X. P., et al. (2010). Lithofacies palaeogeography of the late permian wujiaping age of Sichuan Basin. *J. Palaeogeogr.* 12, 164–176. doi:10.1017/S0004972710001772
- Tribouillard, N., Algeo, T. J., Baudin, F., and Riboulleau, A. (2012). Analysis of marine environmental conditions based on molybdenum-uranium covariation-Applications to Mesozoic paleoceanography. *Chem. Geol.* 324–325, 46–58. doi:10.1016/j.chemgeo.2011.09.009
- Wang, D. W., Luo, X. P., Wu, C. R., and Xu, G. S. (2014). Geochemical characteristics of devonian-permian shale in xiangdongnan depression, hunan, China. *J. Chengdu Univ. Technol. Sci. and Technol. Ed.* 41, 78–86. doi:10.3969/j.issn.1671-9727.2014.01.10
- Wang, Z. P., Zhang, J. C., Sun, R., Liu, C. W., Du, X. R., and Lu, Y. Y. (2015). The gas bearing characteristics analysis of the Longtan Formation transitional shale in well Xiye 1. *Earth Sci. Front.* 22, 243–250. doi:10.13745/j.esf.2015.02.022
- Wedepohl, K. H. (1971). Environmental influences on the chemical composition of shales and clays. *Phys. Chem. Earth* 8, 307–333. doi:10.1016/0079-1946(71)90020-6
- Wedepohl, K. H. (1991). "The composition of the upper Earth's crust and the natural cycles of selected metals," in *Metals and their compounds in the environment*. Editor E. Merian (Weinheim: VCH-Verlagsgesellschaft), 3–17.
- Yan, D. T., Chen, D. Z., Wang, Q. C., and Wang, J. G. (2010). Large-scale climatic fluctuations in the latest Ordovician on the Yangtze block, South China. *Geology* 38, 599–602. doi:10.1130/g30961.1
- Zhang, J. K., He, S., Yi, J. Z., Zhang, B. Q., Zhang, S. W., Zheng, L. J., et al. (2014). Rock thermo-acoustic emission and basin modeling technologies applied to the study of maximum paleotemperatures and thermal maturity histories of Lower Paleozoic marine shales in the western Middle Yangtze area. *Acta Pet. Sin.* 35, 58–67. doi:10.7623/syxb201401006
- Zhang, Y., Liu, X. P., Dong, Q. Y., Ding, W. X., Li, H. D., Liu, S. L., et al. (2013). Formation conditions and favorable exploration zones of shale gas in Upper Permian Longtan Formation of Subei area. *J. Oil Gas Technol.* 35, 36–40. doi:10.3969/j.issn.1000-9752.2013.03.008
- Zhao, Z. J., Zhou, H., Chen, X., Liu, Y. H., Zhang, Y. B., Liu, Y. E., et al. (2012). Sequence lithofacies paleogeography and favorable exploration zones of the Permian in Sichuan Basin and adjacent areas, China. *Acta Pet. Sin.* 33, 35–51. doi:10.7623/syxb2012S2004
- Zhou, D. S., Xu, L. F., Pan, J. P., and Huang, X. W. (2012). Prospect of shale gas exploration in the upper permian longtan Formation in the Yangtze massif. *Nat. Gas. Ind.* 32, 6–10. doi:10.3787/j.issn.1000-0976.2012.12.002